

The young stellar population of IC 1613. III. New O-type stars unveiled by GTC-OSIRIS. [★]

M. Garcia^{1,2} and A. Herrero^{1,2}

¹ Instituto de Astrofísica de Canarias, C/ Vía Láctea s/n E-38200 La Laguna, Tenerife, Spain.
e-mail: mgg@iac.es

² Departamento de Astrofísica, Universidad de La Laguna, Avda. Astrofísico Francisco Sánchez, s/n, E-38071 La Laguna, Tenerife, Spain.

Received July, 2012; accepted November 16th, 2012

ABSTRACT

Context. Very low metallicity massive stars are key to understand the reionization epoch. Radiation-driven winds are one of the main agents of the evolution of massive stars, and consequently an important ingredient of our models of the early-Universe. Recent findings hint that the winds of massive stars with poorer metallicity than the SMC may be stronger than predicted by theory. Besides calling the paradigm of radiation driven winds into question, this result would impact the calculated ionizing radiation and mechanical feedback of massive stars, and the role these objects play at different stages of the Universe.

Aims. The field needs a systematic study of the winds of a large sample of very metal poor massive stars. The sampling of spectral types is particularly poor in the very early types. This paper's goal is to increase the list of known O-type stars in the dwarf irregular galaxy IC1613, whose metallicity is smaller than the SMC's by roughly a factor 2.

Methods. Using the reddening-free Q-parameter, evolutionary masses and GALEX photometry, we built a list of very likely O-type stars. We obtained low-resolution ($R \sim 1000$) GTC-OSIRIS spectra for a fraction of them and performed spectral classification, the only way to unequivocally confirm candidate OB-stars.

Results. We have discovered 8 new O-type stars in IC1613, increasing the list of 7 known O-type stars in this galaxy by a factor of 2. The best quality spectra were analyzed with the model atmosphere code FASTWIND to derive stellar parameters. We present the first spectral type – effective temperature scale for O-stars beyond the SMC.

Conclusions. The target selection method is successful. From the pre-selected list of 13 OB star candidates, we have found 8 new O-stars, 4 early-B stars and provided a similar type for a formerly known early-O star. Further tests are needed but the presented procedure can eventually make preliminar low resolution spectroscopy to confirm candidates unnecessary. The derived effective temperature calibration for IC1613 is about 1000K hotter than the scale at the SMC. The analysis of an increased list of O-type stars will be crucial for the studies of the winds and feedback of massive stars at all ages of the Universe.

Key words. Stars: early-type – Stars: massive – Stars: fundamental parameters – Stars: Population III – Galaxies: individual: IC1613 – Galaxies: stellar content

1. Introduction

Massive stars are crucial to understand the Universe because of their impact in many astrophysics fields. Mighty stellar winds and ionizing radiation fields, and a violent end as supernova, disrupt their surrounding media and contaminate it with the products of the nuclear reactions that feed these titans. Our interest on very low metallicity massive stars is growing rapidly because of their role in the early Universe. In the primordial extremely metal-poor environment, the formation of high mass stars was favoured (Bromm et al., 2002) and these started the re-ionization of the Universe. Massive stars are suspected progenitors of long gamma ray bursts (long-GRBs Geogry et al., 2009; Woosley & Heger, 2006), and this connection may explain the highest frequency of long-GRBs with higher redshift and decreasing metallicity (Gehrels et al., 2009, and references therein).

Blue massive stars (BMS) experience radiation driven winds, powered by the scattering of photons in numerous UV transitions of metallic ions and therefore strongly dependent on metallicity. Radiation driven winds are one of the central pillars of the current paradigm of massive stars, as the wind removes mass from the star and changes the physical conditions at the stellar core. The wind regulates, directly or indirectly the evolution of the star, its ionizing radiation and mechanical feedback, the supernova (SN) explosion and type of compact object left, and stellar yields (Geogry et al., 2009; Woosley et al., 2002).

Theory predicts a strong correlation between the momentum carried by the wind and the luminosity of the star and metallicity: the wind-momentum luminosity relation (WLR, Kudritzki, Lennon, & Puls, 1995). This relation and its metallicity dependence have been thoroughly characterized both by theoreticians (e.g. Vink et al., 2001) and observations (Mokiem et al., 2007) from the Milky Way (MW) down to the metallicity of the Small Magellanic Cloud (SMC). Very low metallicity BMS are expected to experience weaker winds than SMC stars and much weaker winds than MW stars. However, some recent results are in marked contrast.

[★] Based on observations made with the Gran Telescopio Canarias (GTC), instaled in the Spanish Observatorio del Roque de los Muchachos of the Instituto de Astrofísica de Canarias, in the island of La Palma. Program ID GTC59-11B.

We have found a resolved Luminous Blue Variable star (LBV) of very low metallicity ($\sim 0.2Z_{\odot}$, Herrero et al., 2010) with strong optical P Cygni profiles; an analogous example exists in NGC2366 (Drissen et al., 2001) and similar unresolved cases may exist in more distant galaxies (Pustilnik et al., 2008; Izotov et al., 2011). Tramper et al. (2011) reported 6 stars with stronger wind momentum than expected at the poor metallicity of their host galaxies ($\sim 1/7Z_{\odot}$) from X-Shooter spectroscopic analyses, although error bars are too large for results to be determinant. Our analysis of an Of star in IC 1613 (Herrero et al., 2012) concluded that the star may have a strong wind or, alternatively, a slower than expected wind acceleration. Lucy (2012) argues that the neglect of wind clumping may explain these findings, but also suggests that the discrepancy may be caused by an additional wind-driving mechanism operating only at certain metallicities, temperatures and luminosities, or negligible in the Galactic counterparts. Herrero et al. (2012)'s and Tramper et al. (2011)'s examples, if confirmed by the detailed study of a large sample of objects, pose a challenge to the standard theory of radiation line-driven winds, as there are few metals to drive the wind. Yet, this might explain why long-GRBs (typically associated with type Ic SN, Woosley & Heger 2006) are mostly found in metal-poor environments (Modjaz et al., 2008; Levesque et al., 2010) but require a strong wind to remove the H and He envelope in the pre-SN stages.

Besides the wind mechanical energy, the ionizing radiation emitted by massive stars is a chief interface of the pre-SN stages with the interstellar medium. The production of ionizing photons can be estimated to first order from the effective temperature (T_{eff}), making T_{eff} vs spectral type calibrations a very useful tool. While the temperature scale for the Milky Way and the Magellanic Clouds have been addressed by a number of works (e.g. Garcia & Bianchi, 2004; Martins et al., 2005b; Massey et al., 2009), no characterization for lower metallicity environments exists.

In order to study very metal-poor BMSs we need to reach out into the Local Group, beyond the Magellanic Clouds (Garcia et al., 2011). IC1613 is the closest Local Group galaxy (DM=24.27 Dolphin et al. (2001); $E(B-V)=0.02$ Lee et al. (1993)) with on-going star formation and poorer metallicity than the SMC: $\sim 0.13Z_{\odot}$ from B-supergiants (Bresolin et al., 2007), $\sim 0.05Z_{\odot}$ from nebular studies (Bresolin et al., 2007; Peimbert et al., 1988; Talent, 1980; Davidson & Kinman, 1982). Bresolin et al. (2007) published a catalog of about 40 OB-stars in this galaxy, found from VLT-FORS2 MOS observations, but it only lists 6 O-types (4 of them were observed and analysed by Tramper et al. (2011)). These, together with the Of star analyzed in Herrero et al. (2012) makes a total of 7 O-type stars known in IC1613, insufficient for a statistical characterization of the WLR at very low metallicities.

It is necessary to extend the sample of known O-stars in IC1613, but so far low-resolution spectroscopy is needed to unequivocally confirm O-candidates. In this paper we present new OB-stars in IC1613 found from low-resolution spectra taken with the Gran Telescopio Canarias (GTC). The targets were selected using a set of photometry-based criteria which works well for O-stars as endorsed by the derived spectral types. This work is part of our study of the BMS population of IC1613 and uses the photometric catalog and study of OB associations published in Garcia et al. (2009, hereafter GHV09) and Garcia et al. (2010, hereafter GHC10). All stellar identification numbers refer to the GHV09 catalog, unless otherwise specified.

We present the target selection procedure optimized for O-type stars in Sect. 2. The observations and data reduction are

detailed in Sect. 3. In Sect. 4 we provide spectral types for the targets, and in Sect. 5 we derive their stellar parameters. Finally, our conclusions are provided in Sect.6.

2. Target Selection

O-type stars cannot be chosen solely from optical photometry, since their colors are very similar to those of the slightly cooler B-types. So far spectral types are needed to unequivocally spot out O-stars, but this may be costly in observing time since they are often obscured by gas and dust and quite faint. We therefore need to devise a method to produce a sound list of very likely O-type stars, and additional criteria (besides photometric colors) are needed to this end.

GHV09 showed that OB-stars are found in a particular locus of the U-B vs Q diagram (see Fig. 1 and GHV09-Fig. 5), Q being the reddening-free Q pseudo-color $Q = U - B - 0.72 \times (B - V)$. The explanation is that Q increases monotonically towards later spectral types in the interval $Q \in [-1.0, -0.4]$, corresponding to O3-A0 types (see e.g. the calibration of Fitzgerald (1970), and GHC10). While Q is an indicator of spectral type, U-B holds the information of whether the star is reddened or not. Q is the primary target selection criterion: starting from a catalog with small photometric errors ($<0.05\text{mag}$) to minimize the impact on Q, we choose "blue-Q" stars with $Q < -0.8$. An additional advantage of choosing stars mainly from their Q pseudo-color instead of classical B-V cuts, is that locally reddened targets are not discarded (see Fig. 2).

Yet, in order to separate O and B stars (see GHV09) further information is needed. From IC1613's "blue-Q" stars, we chose those with the largest evolutionary mass ($> 25 M_{\odot}$, derived by GHC10) that matched stellar-like sources in GALEX-FUV images. We allowed for magnitudes as faint as $V = 19.8$ as long as the GALEX detection is clear.

The procedure is not free of caveats. From its definition it follows that the Q-parameter depends on the adopted reddening law and is subject to larger photometric errors than individual filters. Besides, some O stars exhibit $Q > -0.8$ and would not be included in the current selection. Nonetheless, our selection criteria make the hunt for O-type stars more effective.

The list of candidate OB-stars and their photometry is provided in Table 1. We also included in the spectroscopic follow-up two objects with colors similar to the known WO and LBV-candidate stars in IC1613 respectively (see GHV09), one previously known O star (65426, O5-6 V, Bresolin et al. (2007)), and two additional blue but fainter stars that serendipitously fell in-slit. Their location in IC1613 is shown in Fig. 3. Figs. 1 and 2 illustrate their position in the U-B vs Q and color-magnitude diagrams. Finding charts are provided in Appendix A.

3. Observations and data reduction

The observations were carried out with the Optical System for Imaging and low Resolution Integrated Spectroscopy (OSIRIS) at the 10m-telescope GTC. The program was granted 5 hours under proposal GTC59-11B (P.I. M.Garcia), in service mode. The observations consisted on long-slit spectroscopy taken with the R2000B VPH and 1.2" slits. The spectra cover the $\sim 4000\text{-}5500 \text{ \AA}$ range with resolving power $R \sim 1000$, suitable to perform spectroscopic classification. The spectra are well oversampled (about 5 pixels) and can be rebinned to improve the signal-to-noise ratio (SNR).

Table 1. Coordinates, photometric data and association membership for the sample stars, from GHV09. Stars not belonging to any OB association are marked [-1] in column ASSOC. The spectral types provided in column SpT were derived in this work.

ID	RA[deg] J2000.0	DEC[deg] J2000.0	ASSOC	V	B-V	Q	SpT	Notes
64066	16.258634	2.157802	147	19.03	-0.21	-0.97	O3 III(f)	
65426	16.262785	2.167927	162	19.62	-0.20	-0.91	O6 III	offslit, O5-6 V (Bresolin et al., 2007)
69476	16.277063	2.158948	185	18.89	-0.22	-0.97	O6.5 III	
36611	16.186651	2.109095	44	19.46	-0.13	-0.91	O7 III-V	multiple?
75661	16.307566	2.139771	197	19.79	0.18	-1.07	O8 III	
67684	16.270335	2.159043	175	19.02	-0.21	-0.91	O8.5 I	composite?
60782	16.249088	2.153501	127	19.61	-0.22	-0.91	O9.5 III	blend?
61331	16.250685	2.153629	127	19.14	-0.21	-0.85	O9.7 II	elongated shape but single detection in GHV09
71708	16.286754	2.152986	192	19.78	-0.02	-1.04	lateO III+neb	
60269	16.247649	2.153412	127	20.49	-0.29	-0.82	B0.5 I	offslit
60882	16.249384	2.096583	135	19.44	-0.14	-0.84	B0.5 I-III	
27381	16.163216	2.146994	-1	18.42	-0.07	-0.83	B1-1.5 I	
35071	16.182901	2.084464	-1	18.78	0.65	-0.99	B2.5 III	V39-like colors. Double?
44736	16.206282	2.106804	56	19.89	-0.12	-0.81		offslit
67063	16.268118	2.163212	176	19.65	-0.04	-0.96		
68456	16.273197	2.153952	175	21.67	0.19	-1.35		WR-candidate

Table 2. Observation log: slit position angles (PA), included targets, date of observations, seeing and transparency conditions, fraction of illuminated moon and airmass.

Slit	PA [deg]	Stars	Date	Seeing ["]	Trans.	Moon [FLI]	Airmass
slit_a	85.6	61331, 27381, 60269, 60782	10-02-2011	0.9	Spect.	0.40	1.15
slit_b	-57.8	69476, 71708, 75661, 65426	10-24-2011	1.2	Clear	0.05	1.12
slit_c	45.85	64066, 35071, 44736	09-17-2011	0.9	Clear	0.70	1.24
slit_d	-28.6	67684, 67063, 68456	09-16-2011	0.9	Clear	0.80	1.44
slit_e	-78.8	36611, 60882	09-17-2011	1.0	Clear	0.70	1.66 ^a

^(a) Morning twilight started few minutes before completing the second exposure

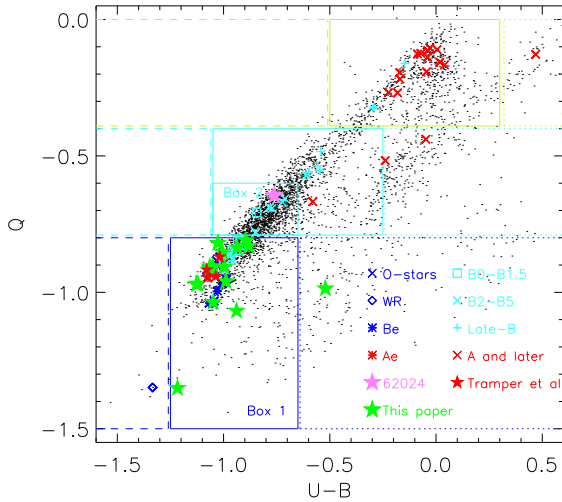


Fig. 1. IC1613's U-B vs Q diagram. Black dots mark catalog stars with high quality photometry from GHV09. Other colors and symbols, except for filled stars, mark the position of stars with known spectral types from Bresolin et al. (2007). O- and early-B- stars concentrate in boxes 1 and 2. The pink star represents 62024, an Of star analyzed by Herrero et al. (2012). Red stars represent the sample of Tramper et al. (2011) in IC1613. Green stars mark this paper targets.

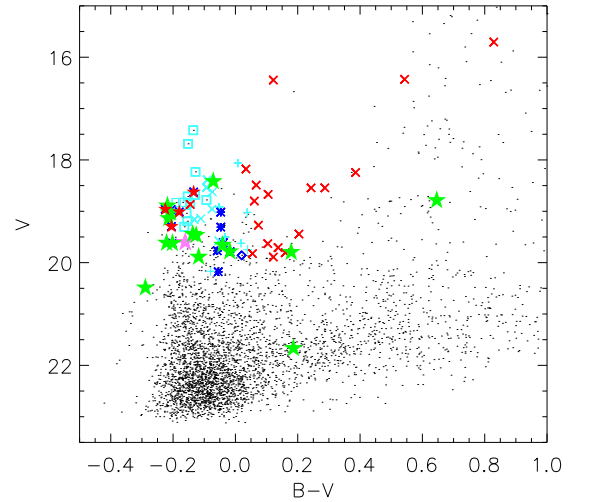


Fig. 2. IC1613's color-magnitude diagram. Colors and symbols as in Fig. 1. OB-stars are dispersed in the color-magnitude diagram, and do not concentrate on the galaxy's blue-plume. In sight of this diagram three targets are remarkably reddened, and would have been discarded with classical $B - V$ color cuts. Note also that the brightest stars of the blue-plume are early-B supergiants.

The slits were oriented in specific angles to include several targets. One 1-hour long Observing Block (OB) was devoted to each slit. The observing conditions are compiled in Table 2.

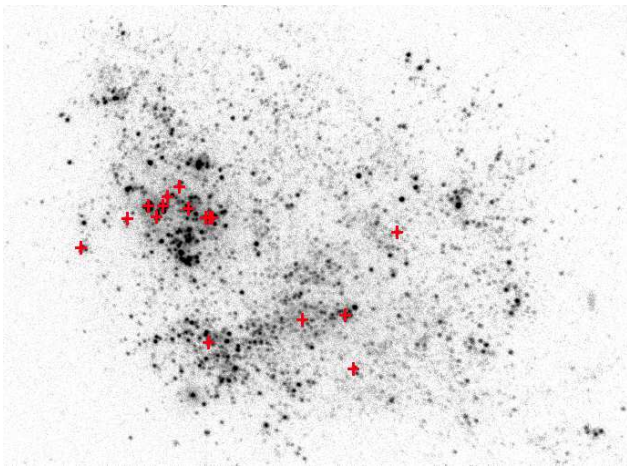


Fig. 3. IC1613, GALEX’s FUV-channel. North is up and East is left. Plus symbols mark the position of the sample stars, chosen with the following criteria: Blue Q-parameter ($Q < -0.8$), V-magnitude ($V < 19.8$), intense emission in GALEX images, large evolutionary mass ($M > 25M_{\odot}$) and no H_{α} emission whenever possible.

3.1. Data reduction

Reduction was performed according to standard IRAF¹ procedures. Each slit OB was split into two 1249s exposures, to enable cosmic ray removal. The exposures were coadded prior to any reduction procedure (case-A), with the *imcombine* routine and the *crreject* mechanism for cosmic-ray rejection. We checked against displacement between consecutive exposures and found shifts of up to 7 pixels in extreme cases (slightly larger than 1 resolution element) in the spectral direction. For this reason we also reduced the individual exposures of all stars separately, and coadded the two spectra at the end of the reduction (case-B), to avoid problems with wavelength shifts. We compared the resulting spectra from case-A and case-B reduction and found undetectable differences, with a better cosmic-ray extraction in case-A, which we adopt.

The *ccdproc* routine was used to trim the images and remove vignetted areas of the CCD, and also for bias subtraction and flat-field correction. The bias correction was performed using the overscan region. Each spectrum was flat-field corrected with the normalized attached daytime flats for that OB. After checking against shifts between the master arcs provided by the observatory and the attached arcs, the former were used for wavelength calibration because of their increased SNR. A 2-D wavelength calibration solution was obtained and assigned to the data using iraf routines *identify*, *reidentify*, *fitcoords* and *transform*.

We note that the arc lamp image displays diffuse light on the right part of chip-1 at $\lambda \gtrsim 5500\text{\AA}$, and the red wavelength calibration for stars whose spectra laid in this region of the CCD is not reliable. The GTC observatory also reported intermittent technical problems with OSIRIS’s active collimator during the dates of the observations, which may affect the stability of the wavelength calibration. Both factors could explain the wavelength calibration problem reported in Sect. 5. However, neither of them hamper the identification of spectral lines or the deriva-

tion of stellar parameters, hence have no negative impact on this paper goals.

The *apall* task was used for target extraction and background subtraction. Background subtraction was complicated since a fraction of the targets were located in crowded regions, and some of them also experienced nebular contamination. The fit to background levels was performed at the physical line of the image equivalent to 4500\AA , free from nebular transitions. If two stars were very close together, their *apall* aperture was chosen to minimize contamination from the neighbor. Some targets exhibit a pedestal in the transversal cut, which could be caused by either nebular contamination or crowding. We checked H_{α} images to evaluate the first option and, in the event of H_{α} detection, the sky aperture was chosen close to the star, at the pedestal. If there was no H_{α} detection, then we interpreted that the plateau had stellar origin, and the sky contribution was chosen far from the pedestal.

Finally, the R2000B VPH of GTC-OSIRIS experiences a ghost image, with negligible number of counts in the science or arc images. However, a non-negligible structure remains in the flat-field after normalization, which is transmitted to the science image after the flat-field correction. The ghost position varies between different flat-field images, but we have made a conservative estimate of the wavelength ranges that may be affected: $4738 - 4778\text{\AA}$ (chip1) and $4736 - 4784\text{\AA}$ (chip2).

The reduced stellar spectra are shown in Figs. 4 to 5.

4. Spectral Classification

Spectral classification was made after Walborn & Fitzpatrick (1990)’s and Lennon et al. (1992)’s criteria for Milky Way stars bearing in mind metallicity effects, as explained in Castro et al. (2008) and summarized in Castro (2010). As far as we know, no spectral classification criteria exists for metallicity smaller than the SMC. We avoided diagnostics involving simultaneously metallic and non-metallic lines as much as possible. They may be misleading due to the different metallicity of IC1613 and the MW. Spectral subtypes for O-stars were derived comparing mainly the ratios of the lines HeII4541/HeI4471, HeII4200/HeI+HeII4026, HeII4541/HeI4387 and HeII4200/HeI4144, and luminosity class from the HeII4686 line and the SiIV4089/HeI4121 ratio. The main diagnostics for B spectral subtypes were SiIV4089/SiIII4552, MgII4481/HeI4471, SiIII4552/SiIII4128, SiIII4552/MgII4481 and SiII4128/HeI4121, and for luminosity class SiIV4089/HeI4121 and SiIII4552/HeI4387. As the luminosity criteria often involve the undesired He-to-metal ratio, we checked that the observed visual magnitude, corrected from extinction, agrees with the calibrated for the assigned luminosity class. The spectral classifications are provided in Table 1.

The main sources of uncertainty are poor SNR, poorly removed or over-subtracted nebular contamination, unremoved cosmic-rays (exposure times were long and only 2 exposures per target were taken) and the difficult normalization around H_{δ} , that affects all diagnostics involving SiIV4089 and HeI4121. Additionally, the increased background levels of the OBs executed in bright time hamper the detection of the weakest spectral lines; it is possible that weak HeII lines are not detected in actual late-O stars, resulting in a bias towards B-types.

We estimate that spectral types are uncertain by about 1-2 sub-types, depending very much on the SNR of the spectrum and the nebular contamination. Nonetheless we are confident on the O and B classification: HeII lines are clear in the O-types, HeI

¹ IRAF is distributed by the National Optical Astronomy Observatory, which is operated by the Association of Universities for Research in Astronomy (AURA) under cooperative agreement with the National Science Foundation

and Si lines are clear in the B-types, and all the spectra show stellar wings in the Balmer lines. As we have pointed out, the only risk in this sense is that early-B stars may actually be late-O stars with very weak HeII lines, undetected due to high background levels.

From the maximal discovery expectation of thirteen new O-type stars, we have found eight O-stars and three early-B stars, and provided a similar spectral type for the formerly known early-O star 65426. 35071, whose colors were similar to the LBV-candidate V39, turned out to be an additional B-type star.

The observations did not produce spectra apt for classification for the three remaining stars. 68456, located close to IC1613's WO in the U-B vs Q diagram, is dominated by nebular lines with no trace of WR's typical broad wind emissions. 44736 and 67063 exhibit Balmer lines, and seem to also show HeI lines, but the spectra are too noisy for classification.

4.1. Notes on individual targets:

64066 (O3 III(f)): The star displays strong HeII lines whereas HeI lines can be hardly seen. The spectrum also exhibits stellar Balmer wings with intense nebular lines at the core. We examined the subtracted sky spectrum and concluded that it seems unlikely that the absence of HeI lines is caused by nebular contamination. Since NIII4634-40-42 is weak in emission, the star is classified as O3III(f). There may be emission of NIV4058 in the spectrum which would render the star an ((f*)), and also of CIII4647-50-51; however, the SNR is too poor to be conclusive. 64066 is very close to the O9 V star 63747, ~0.5mag fainter, but contamination is unlikely given the absence of HeI lines in the spectrum of 64066.

65426 (O6 III): This target is located inside nebulosity, and the [OIII] lines indicate incomplete sky subtraction. The star displays broad stellar Balmer wings with strong nebular lines at the core. However, HeI lines do not seem contaminated by the nebula. HeII4686 has an artificial P Cygni-like profile caused by a strong cosmic-ray in one of the exposures. We only consider the absorption part of the line. The star was previously classified as O5-6 V by Bresolin et al. (2007), but we find a slightly later spectral type and higher luminosity class, O6 III.

69476 (O6.5 III): The star is located inside GS1 (Meaburn et al., 1988), one of the large bubbles of the galaxy, and the sky subtraction is problematic. The [OIII]5007 line indicates a slight sky undersubtraction while the profile of the Balmer lines at the core hint that the nebular contribution has been oversubtracted. HeI4387 may also experience nebular contamination, but other HeI lines seem free from nebulosity. The HeII lines are broader than HeI. There may be emission of NIII4634 and CIII4647-50-51, which would render the star an ((fc)) type, but SNR is too poor to be conclusive.

36611 (O7 III-V): This star was observed in bright time and almost at twilight, which explains the comparatively poor SNR of its spectrum. The [OIII] lines indicate severe nebular contamination, and the spectrum displays strong nebular lines at the core of the stellar Balmer lines. The HeII lines are broader than the HeI lines and seem to have substructure. The GHV09 catalog has two very close sources about 1'' to the SW, which are fainter by 0.8 and 2.3 magnitudes. We mark 36611 as possibly multiple.

The P Cygni-like shape of HeI4471 is caused by a not totally removed cosmic ray in one of the exposures. HeII4686 is a bit stronger than HeII4541 indicating class-V, but the SiIV4089/HeI4121 ratio suggests class-III. The star's absolute magnitude, if single, is also consistent with an intermediate luminosity class.

75661 (O8 III): The normalization of this star is very problematic and hampers spectral classification. The [OIII]5007 nebular emission indicates that the nebular extraction was not complete. The spectral diagnostics disagree: the HeII4686/HeII4541 ratio clearly indicates that the star has spectral type earlier than O8, but HeII4541/HeI4471, HeII4200/HeI4144 and HeII4200/HeI4026 point towards later spectral types. There seems to be MgII4481 in the spectrum. The weak HeII4686 could be due to a relatively strong wind filling the line, which would agree with the relatively weak H β line. The assigned type is a compromise of these pieces of evidence but the possibility that the star is a binary, specially considering the difficulties in determining its radial velocity, is high. The assigned radial velocity -250km s⁻¹ matches well HeII4541, HeII4686, H β , HeI4922 and HeI4387, but H γ , HeI4471 and HeII4200 indicate vrad=-350km s⁻¹. The luminosity class was derived extrapolating criteria from the earlier O6 types; the star's absolute magnitude is close to the value calibrated for O8 supergiants by Massey (1998).

67684 (O8.5 I): The [OIII] lines in absorption indicate that the sky was oversubtracted, which explains the strong artificial absorption at the core of the Balmer series. The spectral SNR is poor, as the star was observed at large airmass and bright time conditions. The normalization of the spectrum was problematic and hinders spectral classification; He lines are apparently found in broad bands with overlapped narrow lines. HeII4686 looks asymmetric and with several components. The spectral SNR prevents us from deciding whether this is an artifact from normalization or the star is multiple or actually a compact cluster. Nonetheless HeII4686 and HeII4200 are strong. We mark it as possibly composite spectrum.

60782 (O9.5 III): The star is located in a region of nebulosity with intense emission in the Balmer lines. The [OIII]5007 line indicates a slight sky oversubtraction. The spectrum may be contaminated by 61331, which is very close and 0.5 mag brighter but 60782's wider Balmer lines and spectral morphology in general suggest otherwise. There is also a nearby star with very similar V-magnitude and Q-color (60794, V=19.64, Q=-0.99), but it should be left out of the slit at the chosen position angle of the observations. During spectral extraction with *apall* additional fainter nearby stars were detected.

SiIV4089 is blended with H δ difficulting luminosity classification.

61331 (O9.7 II): The star is located in a region of nebulosity with intense emission in the Balmer lines. The [OIII]5007 nebular line indicates sky oversubtraction, which explains the artificial absorption at the core of the Balmer lines. The apparent emission of HeII4541 is due to a cosmic-ray in one of the exposures. The star is very close to 60782 but contamination seems unlikely as the later is 0.5mag fainter. The lines of hydrogen, HeI and HeII yield different radial velocities. The apparent mismatch between HeI and HeII is probably due to a poorly removed cosmic ray in the wing of HeI4471, and the one at HeII4541. The adopted radial velocity was calculated with HeI lines. The HeII4200 line is very weak. The luminosity indicator SiIV4089/HeI4121 suggests class between I and III, hence the assigned class-II. The star's absolute magnitude, calculated from the apparent magnitude corrected by extinction, is also consistent with an intermediate class.

71708 (late-O III + neb.): Spectral quality is too poor to derive radial velocity; IC1613's systemic velocity -234 km s⁻¹ (Lu et al., 1993) is adopted. The spectrum displays broad stellar Balmer wings with strong nebular lines at the core. HeII lines, specially HeII4541 and HeII4686 are clearly seen and indicate

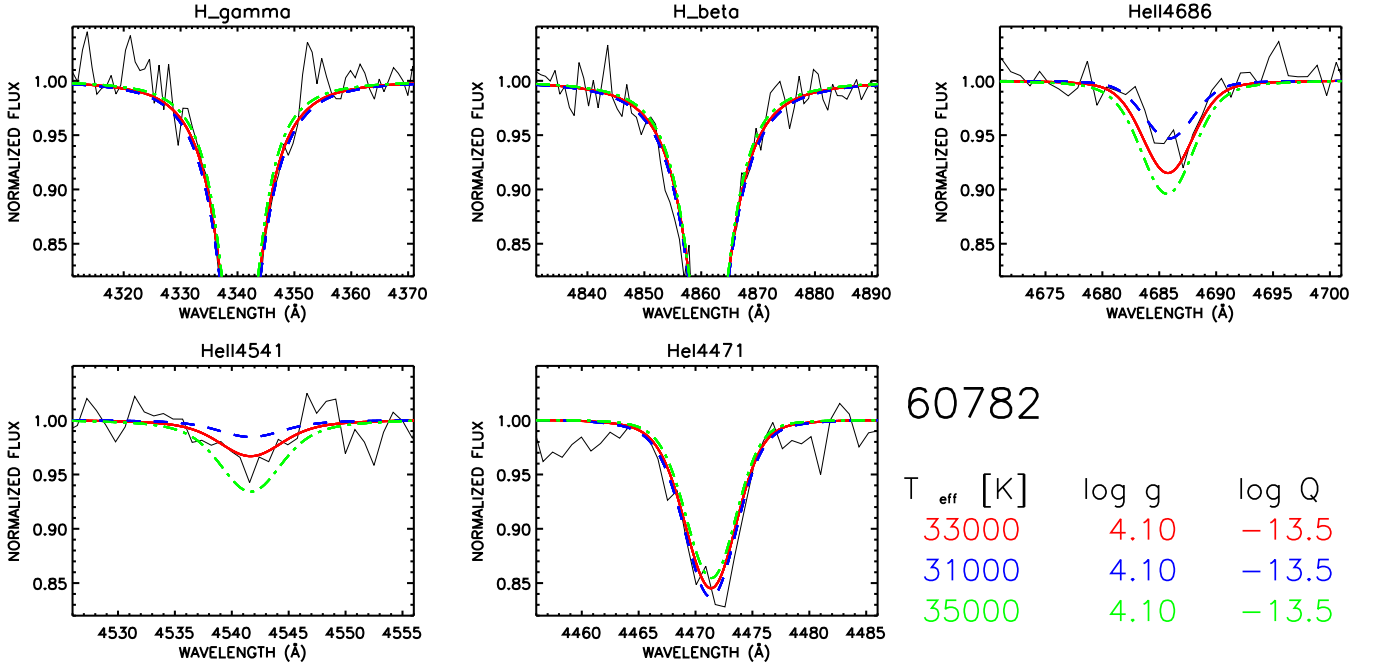


Fig. 6. Best fit FASTWIND model (red, solid line) to sample star 60782 (black). The chart shows the principal diagnostic spectral lines: H_γ and H_β (gravity), HeII4541 and HeII4471 (T_{eff}), and HeII4686 ($\log Q$). To illustrate that T_{eff} is well constrained within the error bars, two additional models (non-solid lines) with T_{eff} varying $\pm 2000\text{K}$ are shown. The fit of these two models to the HeII4541 diagnostic line is poor, defining the error bars for temperature.

an O-type. No spectral type can be assigned, however, since the spectrum displays no stellar HeI lines, very likely due to nebular contamination. SiIII4552 is not seen in the spectrum. HeII4686 is strong in absorption, and stronger than HeII4541; according to the luminosity criteria, this corresponds to luminosity classes III and V for spectral types O8-O9. Its absolute magnitude agrees with the M_V calibrated for a late-O giant (Massey, 1998).

60269 (B0.5 I): The [OIII]5007 line indicates sky oversubtraction, which explains the asymmetry and strong absorption at the core of the Balmer lines. There is a velocity shift between the nebular lines (at IC1613's systemic velocity, measured from the sky spectrum) and the Balmer absorption from the final spectrum. HeI and metal lines experience a smaller shift.

This star was not a primary target of the observing run; it is very faint ($V=20.5$) and consequently its spectrum is noisy. All B-subtype diagnostics point towards an early-B type, but the absence of HeI4121 hints B8-9 types. However, it is possible that HeI4121 is contaminated by nebular emission and this diagnostic was discarded. In absence of HeII4686 and HeI4121 lines, the luminosity class was assigned only from the SiIII4552/HeI4387 ratio, resulting in class-I. However the Balmer lines are too broad for a supergiant: the star may be a late-O type star with undetected HeII lines due to high background level compared to the stellar spectrum signal. Its absolute magnitude ($M_V \lesssim -4$) is consistent with the star being a late-O or an early-B dwarf star, but not with a supergiant ($M_V = -6$). The possibility that its spectrum is contaminated by the very nearby star 60782 (O9.5III) which is 1mag brighter cannot be discarded.

60882 (B0.5 I-III): The [OIII] lines indicate a correct background extraction, although the profiles of the Balmer series core indicate a slight oversubtraction. This star was observed in bright time and almost at twilight, which explains the comparatively poor SNR of its spectrum. No HeII lines can be seen except perhaps HeII4541; the high background level of the exposures could

be hiding the presence of weak HeII lines but the SiIII triplet is strong and suggests a B-type. The SiIV4089/HeI4121 ratio indicates class-I but SiIII4552/HeI4387 suggest class-III.

35071 (B2.5 III): The star seems double at OSIRIS acquisition image, which has enhanced resolution compared to GHV09's INT-WFC catalog. The criteria based on MgII4481, HeII4471 and SiIII4552 point towards types B2.5-3. We note, however, that the presence of SiII4128, expected at this spectral sub-type at higher metallicities, is not clear.

5. Spectroscopic analysis

The resolution and SNR of the dataset enabled a rough determination of the stellar parameters of the sample O-stars. We used synthetic spectra calculated with FASTWIND version 10.1 (Puls et al., 2005) that takes into account line blanketing, non-LTE effects and radiation driven winds, to fit mainly H_γ , H_β , HeII4686, HeII4541 and HeII4471, and secondarily HeII4200, HeII5411, HeI4387 and HeI4922.

The synthetic spectra were taken from a vast grid of FASTWIND models with metallicity $0.13Z_\odot$, computed using the CONDOR facilities at the IAC (Simón-Díaz et al., 2011). $0.13 Z_\odot$ is the equivalent metallicity to the oxygen abundance derived by Bresolin et al. (2007) for B-supergiants in IC1613. The grid covers from 28000 to 55000K, gravity ranging $\log g = 2.6-4.3$ (depending on temperature) and wind-strength Q-parameter $\log Q = M/(v_\infty R_*)^{1.5}$ from -15.0 to -11.7 . The exponent of the wind velocity law β , the helium abundance and the microturbulence also vary in the grid, but were kept constant to typical values for this analysis: $\beta=0.8$, $\epsilon_{He}=0.09$ and $\xi=10\text{km s}^{-1}$.

Starting from effective temperature and gravity ($\log g$) values typical for the star's spectral type, we varied T_{eff} in 1000K steps to fit simultaneously HeII and HeI lines. We then fixed T_{eff} ,

Table 3. Parameters derived for the sample stars

ID	SpT	vrad	T_{eff}	log g	log Q
GHV09		km s^{-1}	K		
64066	O3III((f))	-240	≥ 49000	3.8	-12.7
65426	O6III	-270	40000 ± 2000	3.8	-12.5
69476	O6.5III	-350	37000 ± 2000	3.4	-12.5
36611	O7III-V	-140	40500 ± 3000	4.3	-15.0
75661	O8III	-250	37500 ± 3000	3.9	-12.7
67684	O8.5I	-260	38500 ± 3000	3.8	-15.0
60782	O9.5III	-190	33000 ± 2000	4.1	-13.5
61331	O9.7II	-180	33000 ± 2000	3.8	-15.0

and varied log g in 0.1dex steps to fit the wings of the Balmer lines (the core was discarded since nebular contamination was severe, or unquantifiable, in many cases). The best-fitting gravity value usually requires the recalculation of T_{eff} . Therefore, we iterated this process until all considered spectral lines except for HeII4686 were fitted. The observations do not include H_{α} , but HeII4686 also provides information on the wind. We fitted this line by changing the wind strength log Q parameter. If the wind is not negligible it alters other lines under analysis, and the whole process must be iterated again to adjust temperature and gravity. Only when HeII4686 displays a clearly non-photospheric profile (e.g. asymmetric), we allowed β to vary.

At the spectral resolution of the dataset, rotational and macroturbulent velocities could not be derived unless they are as high as $\sim 250 \text{ km s}^{-1}$. We also measured radial velocities for the targets. We noted some problems with the wavelength calibration, specially in the red part of the spectrum, that affected the HeII5411 line. This cannot be explained by the shifts detected between consecutive exposures, but rather to the reported calibration problems in the red part of some spectra (Sect. 3).

The spectral quality of the dataset enabled the determination of effective temperatures within ± 2000 - 3000 K, as shown in Fig. 6. Typical errors bars for log g are ± 0.2 . We do not quote errors for log Q as the method provides only a rough estimate of the wind influence on other stellar parameters, and the derived values must be considered orientative.

The spectral fit to the sample O-stars is shown in Fig. 7. Results are presented in table 3.

Comments on individual targets

64066 (O3III((f))): This star displays only absorption lines of HeII, with no trace of HeI. We were able to derive only a lower limit for effective temperature. Consequently gravity is also poorly constrained.

69476 (O6.5III): H_{β} could not be used for analysis due to nebular contamination. The helium lines are very broad: we adopted $v_{\text{sin}i} = 250 \text{ km s}^{-1}$. The HeII4541 and HeII4686 lines indicate $v_{\text{rad}} \sim 280 \text{ km s}^{-1}$, but HeI and Balmer transitions yield $\sim 350 \text{ km s}^{-1}$. 69476 is inside the bubble GS1, and the different radial velocities could be artificial and caused by undetected nebular contamination of gas masses moving at different radial velocity than the star. However, we examined the sky spectrum and there seems to be no nebular emission in HeI or HeII lines. Another possible explanation is that the star is a binary. We adopted the radial correction calculated with HeI lines.

60782 (O9.5III): The best fit to HeII4686 would actually require log $Q = -13.0$, but Balmer lines could not be fitted with this strong wind even if log g is increased. Contamination by nearby objects (see Sect. 4.1) could be a possible explanation.

61331 (O9.7II): HeII4686 is blue-shifted and narrow, and is not reproduced by any combination of β and log Q .

5.1. The very low metallicity temperature scale

We present the first sub-SMC temperature scale in Fig. 8. It includes all O-type stars in IC1613 whose effective temperature has been derived from quantitative spectroscopic analysis: the 8 stars analyzed in this paper, plus 5 stars from Tramper et al. (2011) and Herrero et al. (2012). For comparison, we have added temperature determinations of SMC OB-stars from Mokiem et al. (2007) and Massey et al. (2009), and the temperature scale for SMC B-supergiants derived by Trundle et al. (2007). At the same spectral type, the temperatures we derive for IC1613 stars are similar to SMC stars, even though slightly hotter.

We calculated a least squares linear regression to the temperatures of the total sample of analyzed giants and supergiants in IC1613. We proceeded similarly with SMC stars (Mokiem et al. (2007) and Massey et al. (2009)). The high end of IC1613's temperature scale (marked with a dotted line) was not well constrained, since we could only derive a lower temperature limit for the giant O3 of the sample. The other O3 star (from Tramper et al., 2011) is a dwarf and was not considered in the fit. As a test, we discarded the three stars marked as binary/multiple in Table 1 and obtained a very similar temperature scale: uncertain binarity may introduce some scatter in the derived relation but does not change it globally.

The derived scale is ~ 1000 K hotter for IC1613 than for the SMC, as expected given IC1613's poorer metal content. It may be argued whether the difference is significant given the error bars of all points considered: ~ 2500 K in this work vs typically ~ 1000 K, but reaching up to ~ 2000 K for some targets, in Mokiem et al. (2007). It is in our programmed future work to produce a sound temperature scale for IC1613 from enhanced resolution and SNR spectra of a larger sample of stars in this galaxy.

6. Summary and future work

Very low metallicity massive stars are growing more and more important to our understanding of the high-redshift very metal-poor Universe. Current models for the first generations of stars rely on knowledge of present-day massive stars, with radiation driven winds being a main pillar. While the paradigm has been thoroughly tested in the Milky Way and the Magellanic Clouds, recent findings indicate that a different wind driving mechanism may be at work at poorer metallicities. The evolutionary models for population-III massive stars, and the estimates of their ionizing, mechanical and chemical feedback would have to be recomputed. Only the quantitative spectroscopic analysis of a large sample of very metal poor massive stars can shed new light on these topics.

This work uses the 10m telescope GTC as a Local Group explorer, to unveil new OB-type stars in metal poor environments beyond the SMC. From low-resolution long slit spectroscopy, 8 O-stars plus 4 early-B stars have been discovered. The total list of known O-type stars in IC1613 has been increased by a factor of 2. A photometric-based selection method optimized towards O stars has been presented, which will save observing time to similar surveys in other galaxies. The extension of the sample of very metal poor O stars is a fundamental first step to test the theory of radiation driven winds at sub-SMC metallicity.

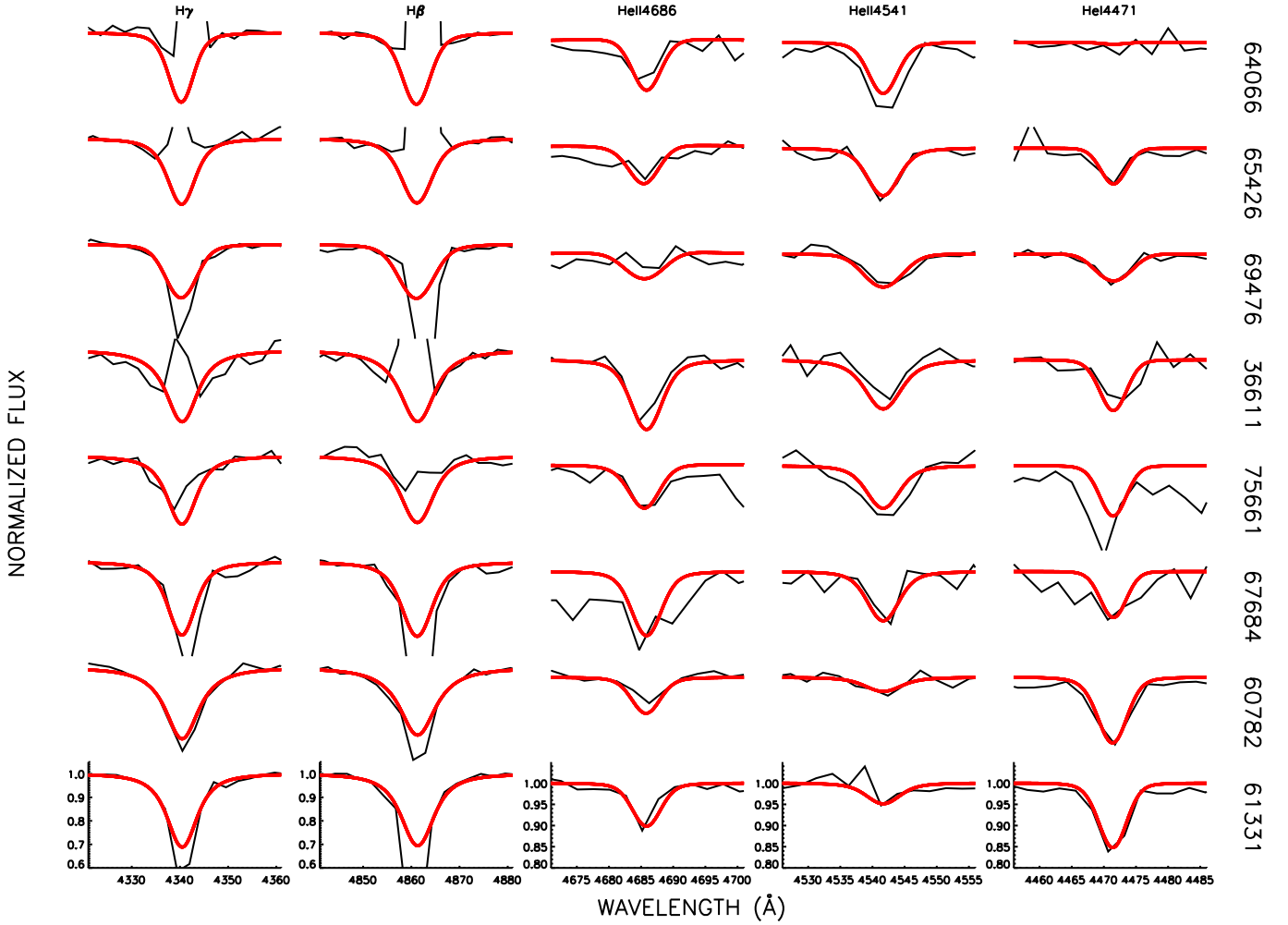


Fig. 7. Best fit FASTWIND model (red) to the sample stars (black). The chart shows the principal diagnostic spectral lines, as in Fig. 6. Stellar identification numbers are provided on the right-hand side of the plot. Axes are provided only for the bottom target for clarity sake; the same axes are used for the remaining stars.

The GTC-OSIRIS spectra were analyzed with FASTWIND models to derive effective temperatures and gravities. From the results we have produced the first temperature scale for O-type stars beyond the SMC. The calibration yields higher temperatures for IC1613 stars, as expected given their comparatively poorer metal content, but must be used with caution given the large error bars of our results.

Follow-up spectroscopy of increased resolution and enhanced SNR is planned for a subset of this paper targets. Its quantitative analysis will provide more accurate stellar and wind parameters, and constraints to the wind theory. The sample will be as extensive as possible in its spectral type and luminosity class coverage so that new clues on the strong wind problems are found. Two interesting by-products will be produced: the first atlas of very metal-poor massive stars and a sound sub-SMC effective temperature calibration.

Acknowledgements. This work has been funded by Spanish MICINN under Consolider-Ingenio 2010, programme grant CSD2006-00070, (<http://www.iac.es/consolider-ingenio-gtc/>), and grant AYA2010-21697-C05-04, and by the Gobierno de Canarias (PID2010119). We would like to thank A. Cabrera-Lavers for fruitful interaction during data processing. This research has made use of Aladin, and also data from the INT telescope (operated by the Isaac Newton Group in the Spanish Observatorio del Roque de los Muchachos). We would like to thank our anonymous referee whose comments helped us to improve this paper.

References

- Bonnarel, F., Fernique, P., Bienaymé, O., et al. 2000, *A&AS*, 143, 33
 Bresolin, F., Urbaneja, M. A., Gieren, W., Pietrzyński, G., & Kudritzki, R.-P. 2007, *ApJ*, 671, 2028
 Bromm, V., Coppi, P. S., & Larson, R. B. 2002, *ApJ*, 564, 23
 Castro, N., Herrero, A., Garcia, M., et al. 2008, *A&A*, 485, 41
 Castro, N. 2010, PhD thesis, Universidad de La Laguna
 Davidson, K., & Kinman, T. D. 1982, *PASP*, 94, 634
 Dolphin, A. E., et al. 2001, *ApJ*, 550, 554
 Drissen, L., et al. 2001, *ApJ*, 546, 484
 Fitzgerald, M. P. 1970, *A&A*, 4, 234
 Garcia, M., & Bianchi, L. 2004, *ApJ*, 606, 497
 Garcia, M., Herrero, A., Vicente, B., Castro, N., Corral, L. J., Rosenberg, A., & Monelli, M. 2009, *A&A*, 502, 1015 [GHV09]
 Garcia, M., Herrero, A., Castro, N., Corral, L., & Rosenberg, A. 2010, *A&A*, 523, A23 [GHC10]
 Garcia M., Herrero A., & Najarro F. 2011, *Ap&SS*, 314
 Gehrels, N., et al., 2009, *ARA&A*, 47, 567
 Georgy, C., et al., 2009, *A&A*, 502, 611
 Herrero, A., et al. 2010, *A&A*, 513, A70
 Herrero, A., et al. 2011, *IAU Symposium*, 272, 292
 Herrero, A., et al. 2012, *A&A*, accepted
 Izotov, Y.I., Guseva, N.G., T.X., Fricke, K.J., & Henkel, C. 2011, *A&A*, 533, A25
 Kingsburgh, R. L., & Barlow, M. J. 1995, *A&A*, 295, 171
 Kudritzki, R.-P., Lennon, D. J., & Puls, J. 1995, In: Walsh J.R., Danziger, I.J. (eds.) *Science with the VLT*. Springer Verlag, p246
 Lee, M. G., Freedman, W. L., & Madore, B. F. 1993, *ApJ*, 417, 553

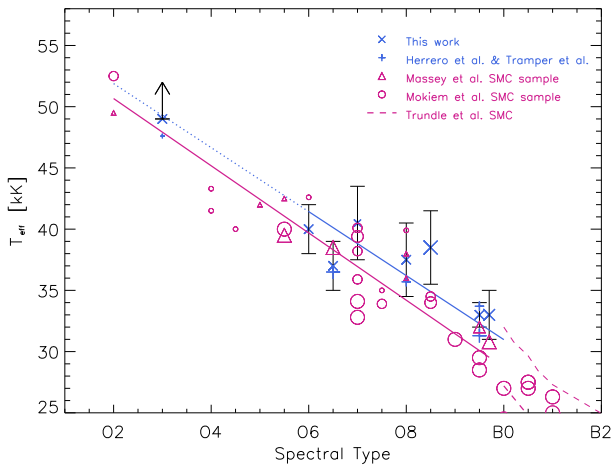


Fig. 8. Very low metallicity temperature scale for O- and early-B stars, including this paper's results and the stars analysed by Tramper et al. (2011) and Herrero et al. (2012) in IC1613. Different symbol size indicates different luminosity class (smallest symbols = class V, largest symbols = class I). For comparison, we have included derived temperatures for OB-stars in the SMC from Mokiem et al. (2007) and Massey et al. (2009) (violet), and Trundle et al. (2007)'s calibration for SMC B supergiants (dashed-thick) and dwarfs (dashed-thin). Solid lines represent linear regressions to the joint sample of O-giants and supergiants in the SMC (violet) and IC1613 (blue). The high end of the temperature scale in IC 1613 is not well constrained, hence marked with a dotted line.

- Lennon, D. J., Dufton, P. L., & Fitzsimmons, A. 1992, *A&AS*, 94, 569
 Levesque, E. M., et al. 2010, *AJ*, 140, 1557
 Lu, N. Y., Hoffman, G. L., Groff, T., Roos, T., & Lamphier, C. 1993, *ApJS*, 88, 383
 Lucy, L. B. 2012, *A&A*, 543, A18
 Martins, F., et al. 2004, *A&A*, 420, 1087
 Martins, F., et al. 2005a, *A&A*, 441, 735
 Martins, F., Schaerer, D., & Hillier, D. J. 2005b, *A&A*, 436, 1049
 Massey, P. 1998, *Stellar astrophysics for the local group: VIII Canary Islands Winter School of Astrophysics*, 95
 Massey, P., Zangari, A. M., Morrell, N. I., Puls, J., DeGioia-Eastwood, K., Bresolin, F., & Kudritzki, R.-P. 2009, *ApJ*, 692, 618
 Meaburn, J., Clayton, C. A., & Whitehead, M. J. 1988, *MNRAS*, 235, 479
 Modjaz, M., et al. 2008, *AJ*, 135, 1136
 Mokiem, M. R., et al. 2007, *A&A*, 473, 603
 Peimbert, M., Bohigas, J., & Torres-Peimbert, S. 1988, *Revista Mexicana de Astronomia y Astrofisica*, 16, 45
 Puls, J., Urbaneja, M. A., Venero, R., et al. 2005, *A&A*, 435, 669
 Pustilnik, S. A., et al., 2008, *MNRAS*, 388, L24
 Simón-Díaz, S., Castro, N., Herrero, A., et al. 2011, *Journal of Physics Conference Series*, 328, 012021
 Talent, D. L. 1980, Ph.D. Thesis
 Tramper, F., et al. 2011, *ApJ*, 741, L8
 Trundle, C., Dufton, P. L., Hunter, I., Evans, C. J., Lennon, D. J., Smartt, S. J., & Ryans, R. S. I. 2007, *A&A*, 471, 625
 Vink, J. S., et al. 2001, *A&A*, 369, 574
 Walborn, N. R., & Fitzpatrick, E. L. 1990, *PASP*, 102, 379
 Woosley, S. E., Heger, A., & Weaver, T. A. 2002, *Reviews of Modern Physics*, 74, 1015
 Woosley, S. E., & Heger, A. 2006, *ApJ*, 637, 914

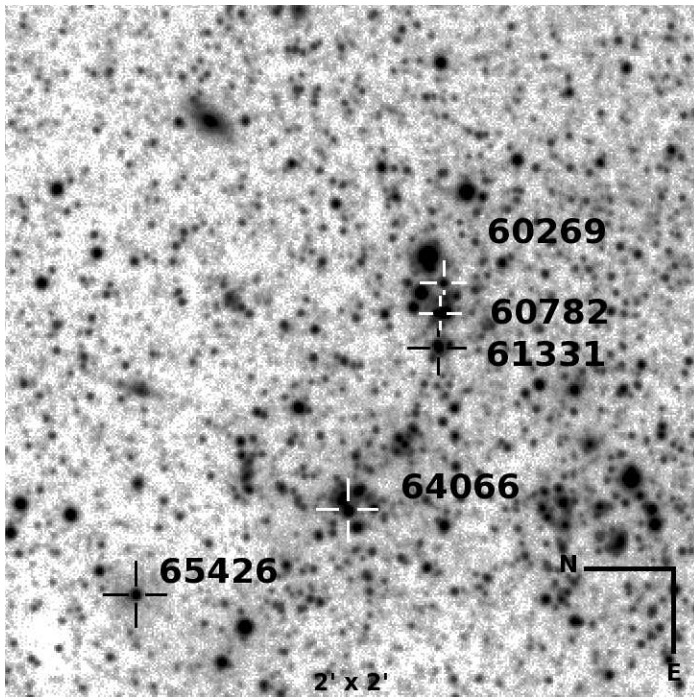


Fig. A.1. Stars 60269 (B0.5 I), 60782 (O9.5 III), 61331 (O9.7 II), 64066 (O3 III(f)) and 65426 (O6 III).

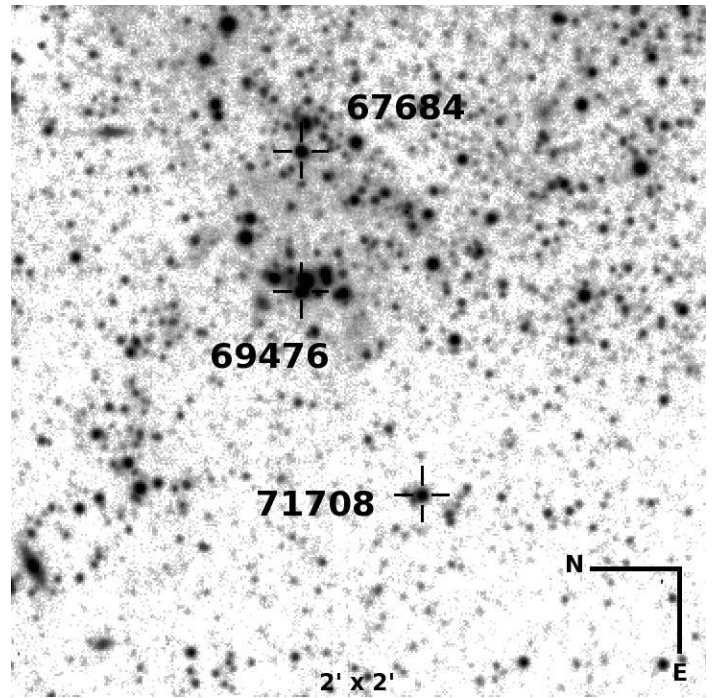


Fig. A.3. Stars 67684 (O8.5 I), 69476 (O6.5 III) and 71708 (late-O III+neb).

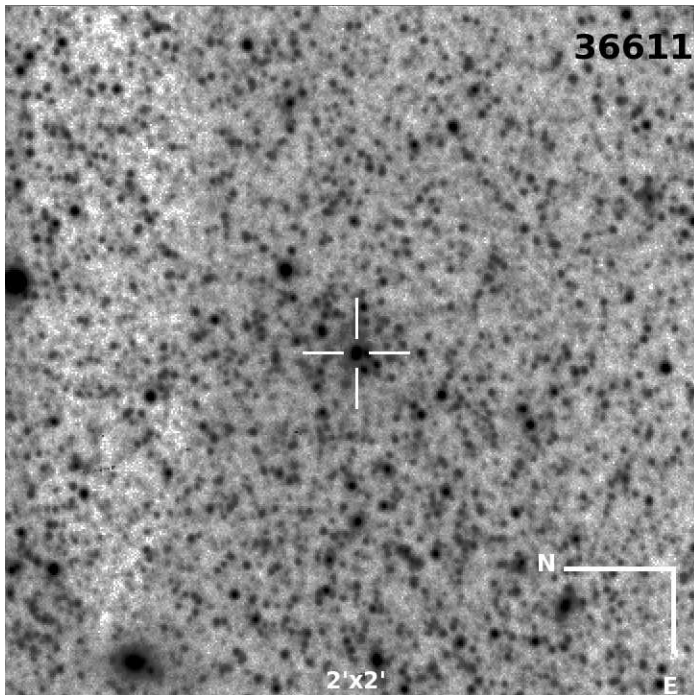


Fig. A.2. Star 36611 (O7 III-V).

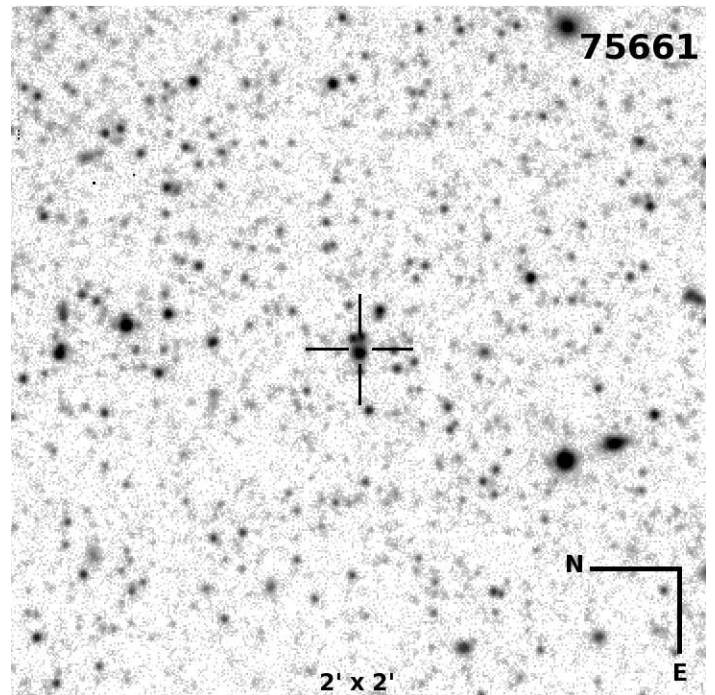


Fig. A.4. Star 75661 (O8 III).

Appendix A: Finding charts for the sample stars

Finding charts for the newly identified OB stars are provided in this section. The images were taken with the Wide Field Camera (WFC) at the 2.5m Isaac Newton Telescope (INT); for more details see GHV09. All the identification charts show a field of $2' \times 2'$, observed with broad Harris V-band filter.

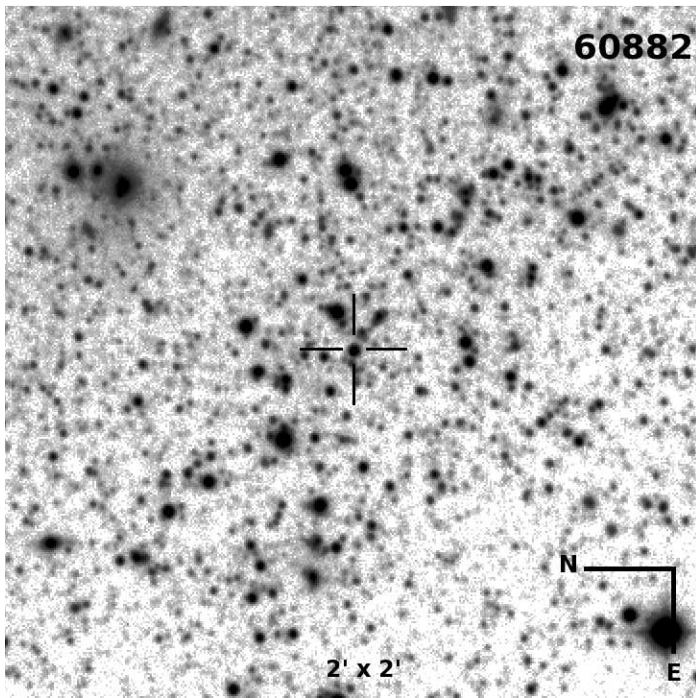


Fig. A.5. Star 60882 (B0.5 I-III).

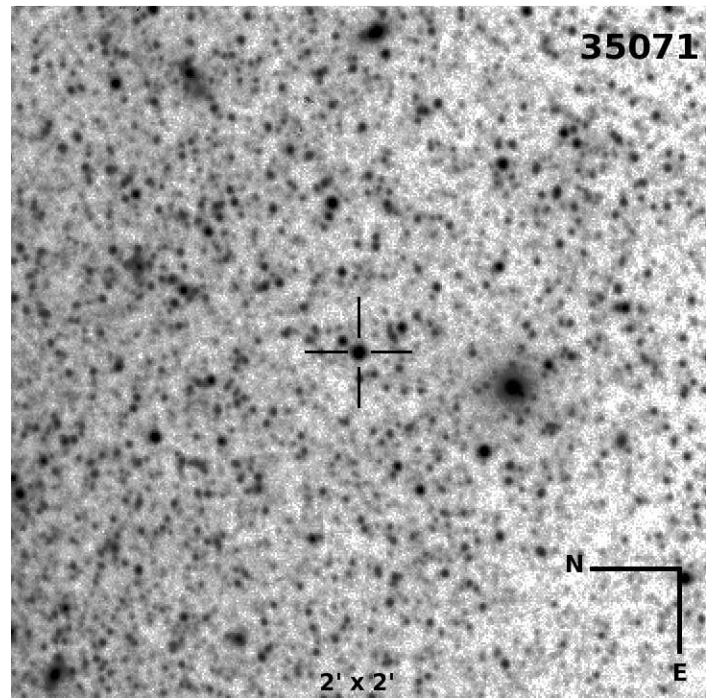


Fig. A.7. Star 35071 (B2.5 III).

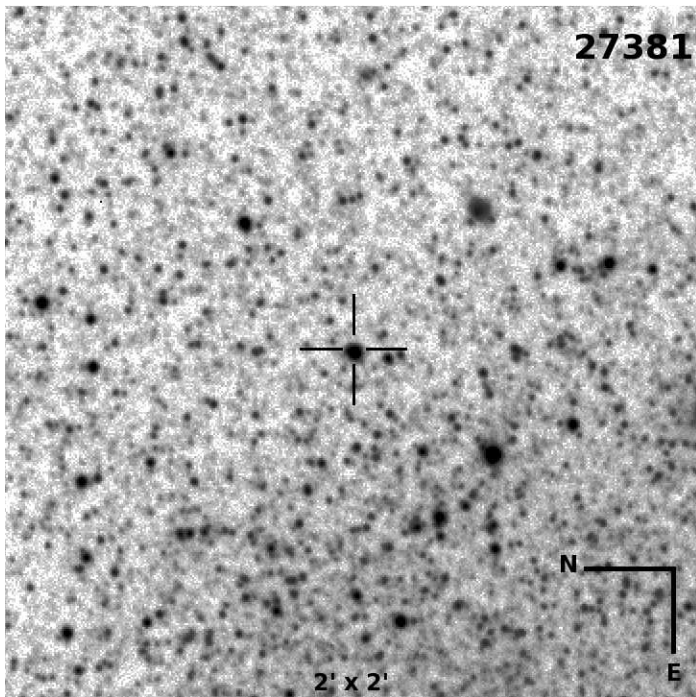


Fig. A.6. Star 27381 (B1-1.5 I).